INTERNATIONAL JOURNAL FOR NUMERICAL METHODS IN FLUIDS, VOL. 12, 625–636 (1991)

EULER ANALYSIS OF TRANSONIC STATOR–ROTOR INTERACTION USING A FINITE VOLUME METHOD

IN-MO KANG AND KEUN-SHIK CHANG

Department of Aerospace Engineering, Korea Advanced Institute of Science and Technology, PO Box 150, Cheongryang, Seoul, Republic of Korea

SUMMARY

A generalized finite volume method that can solve the Euler equations for the stator and rotor parts of stage flow in similar formulations is presented. The method consists of a new moving grid finite volume formulation applied to the rotor region and the existing fixed grid finite volume method used in the stator region, with the data transfer made by an interpolation procedure at the sliding surface in between. The accuracy of the method has been demonstrated on a simple cascade flow before the time-dependent compressor stage flow is fully investigated. The transonic stator–rotor flow interaction is elucidated within the inviscid and rotational flow limit.

KEY WORDS Single-stage compressor Moving grid finite volume method Stator–rotor potential interaction Inviscid wake–rotor interaction

INTRODUCTION

Recently, considerable attention has been given to axial-type compressor and turbine cascade flow problems with stator–rotor interaction. Normally, axial-flow-type turbomachines include closely packed stages of blades, each stage consisting of alternating rotor and stator rows of blades. Work is done on the fluid agent by the action of the rotor blades, some of which is converted to pressure before the flow is redirected to the next rotors by the stator blades.

It has been indicated[1] that the stator–rotor interaction has three distinct causes of unsteadiness. One is the viscous vortex shedding near the trailing edge of the stator blades. Another is the wake–rotor interaction in which the wakes from the stator blades are passed to the downstream rotor blades. The third is the potential stator–rotor interaction in which the pressure disturbance caused by the leading edge part of the rotor blades sweeps upstream all the way to the stator blades. Additional unsteadiness is possibly caused in this case if the flow is viscous, by affecting the vortex-shedding mechanism at or near the stator trailing edges. The present study is based on the formulation of the Euler equations and therefore can take non-viscous phenomena such as the inviscid wake–rotor interaction and the potential stator–rotor interaction into account.

Sometimes turbomachinery is operated in a choked state under off-design conditions. Deliberate introduction of choked flow is also made to the inlet guide vanes, partly for the compression effect and partly for the blockage of upstream noise radiation from the fan or compressors.[2] In the present study we consider the stator–rotor interaction under choked flow conditions.

The existence of moving blades in the present problem causes a computational difficulty, which has been treated in the literature by two distinct approaches. One approach uses relative coordinates in the rotor region,[3,4] introducing moving contact surfaces capable of supporting

0271–2091/91/070625–12$06.00

Received December 1989
Revised May 1990

jumps in the tangential velocity, total enthalpy, etc. In this context, Erdos *et al.*[3] used the MacCormack scheme to solve the inviscid transonic fan stage problem, while Jorgenson and Chima[4] solved viscous turbine flow using an explicit finite difference method. The other approach,[5–8] which is comparable to the one used in the present method, uses identical co-ordinates in both the stator and rotor regions, with the grid-moving effect accounted for in the rotor region. For example, Rai used the finite difference method[5–7] to analyse the inviscid supersonic flow in a rotor–stator configuration as well as viscous turbine stage flows including three-dimensional effects. Oden *et al.*,[8] on the other hand, considered the inviscid supersonic stator–rotor interaction problem using the finite element method formulated with the adaptive grid.

In the present study we have developed a time-accurate, efficient numerical technique based on the finite volume formulation. The Euler equations are solved for two-dimensional compressor stator–rotor stage flow until a fully periodic or quasi-steady state is established in the flow. The stator region is treated with the fixed grid finite volume formulation originated by Jameson *et al.*,[9] while the dynamic rotor region is treated by its modified version developed in the present study. The two regions are juxtaposed through a sliding surface across which data exchange is performed by an interpolation process. This modified formulation was first tested for accuracy on a simple isolated cascade flow before the interactive stage flow problem was fully investigated. The method turned out to be quite efficient in solving the compressible stage flow.

NUMERICAL METHODS

Finite volume formulation

The unsteady two-dimensional Euler equations of conservation law form in rectangular Cartesian co-ordinates (x, y) are

$$\frac{\partial w}{\partial t}+\frac{\partial f}{\partial x}+\frac{\partial g}{\partial y}=0, \tag{1}$$

where

$$w=\begin{bmatrix}\rho\\ \rho u\\ \rho v\\ \rho e\end{bmatrix}, \qquad f=\begin{bmatrix}\rho u\\ \rho u^2+p\\ \rho uv\\ \rho uh\end{bmatrix}, \qquad g=\begin{bmatrix}\rho v\\ \rho uv\\ \rho v^2+p\\ \rho vh\end{bmatrix}, \tag{2}$$

$$e=\frac{p}{\rho(\gamma-1)}+\frac{u^2+v^2}{2}, \tag{3}$$

$$h=e+p/\rho. \tag{4}$$

Here ρ is the density, u and v are the Cartesian velocity components, e is the total internal energy per unit mass, p is the pressure, h is the total enthalpy and γ is the specific heat ratio.

The integral counterpart of equations (1) takes the form, for a fixed finite volume A and its boundary C,

$$\iint_A\left(\frac{\partial w}{\partial t}\right)\mathrm{d}A+\oint_C(f\mathrm{d}y-g\mathrm{d}x)=0. \tag{5}$$

If the control volume is in motion relative to the fixed co-ordinate system (see Figure 1), then additional flux comes into play due to the moving boundaries[10] as in

$$\frac{\mathrm{d}}{\mathrm{d}t}\iint_{A(t)} Q\,\mathrm{d}A=\iint_{A}\left(\frac{\partial Q}{\partial t}\right)\mathrm{d}A+\oint_{C} Q(\boldsymbol{\zeta}\cdot\mathbf{n})\,\mathrm{d}l, \tag{6}$$

where $\boldsymbol{\zeta}$ is the displacement velocity of the boundary element $\mathrm{d}l$. The modified integral form of the governing equations (1) is then

$$\frac{\mathrm{d}}{\mathrm{d}t}\iint_{A(t)} w\,\mathrm{d}A+\oint_{C}[(f-w\xi)\,\mathrm{d}y-(g-w\eta)\,\mathrm{d}x]=0, \tag{7}$$

where ξ and η are the Cartesian components of the displacement velocity $\boldsymbol{\zeta}$. If $\boldsymbol{\zeta}$ is equal to the fluid velocity $\mathbf{V}$, equation (7) simply becomes the Lagrangian form integral equations. For the control volumes in the rotor region undergoing a collective rigid motion as in the present formulation, the integral form (7) can be replaced by the approximation

$$A\frac{\mathrm{d}w}{\mathrm{d}t}+qw=0, \tag{8}$$

where

$$qw=\oint_{C}[(f-w\xi)\,\mathrm{d}y-(g-w\eta)\,\mathrm{d}x]. \tag{9}$$

In the fixed stator grid region, ξ and η are simply replaced by zero.

For a quadrilateral-type finite volume, such as the one designated by (i,j) in Figure 2, a flux quantity through the boundary surface is cell-averaged as

$$w_{12}=(w_{i-1,j}+w_{i,j})/2. \tag{10}$$

The governing equations can then be represented in the form

$$\left.\frac{\mathrm{d}w}{\mathrm{d}t}\right|_{i,j}+\frac{1}{A_{i,j}}qw_{i,j}=0, \tag{11}$$

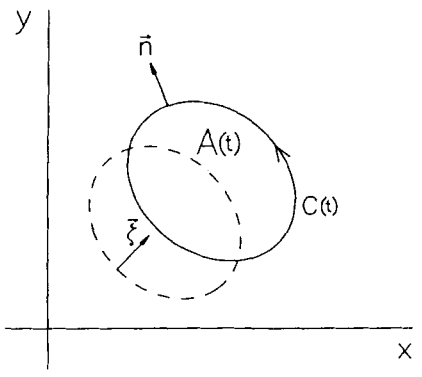

Figure 1. The moving control volume

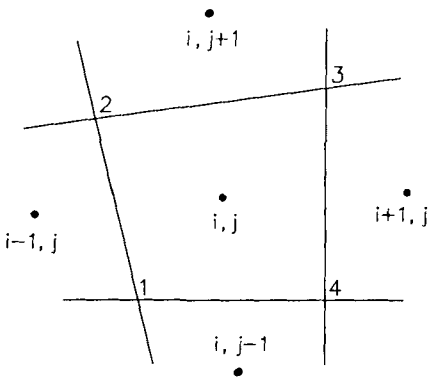

Figure 2. Interior cell structure

where q is a numerical operator similar to the one given by Jameson *et al.*[9] This scheme corresponds to taking central differencing spacewise and is subjected to oscillations and overshoots near the shock wave. To suppress these numerical anomalies, the artificial dissipation terms, dw, are often added to the governing equations[9,11] as follows:

$$\frac{\mathrm{d}w}{\mathrm{d}t}+pw=0, \tag{12}$$

$$pw=\frac{1}{A}(qw-\mathrm{d}w). \tag{13}$$

We now employ the classical fourth-order Runge–Kutta method for the time-stepping procedure:

$$\begin{aligned}
w^0 &= w^n,\\
w^1 &= w^0-\frac{\Delta t}{2}pw^0,\\
w^2 &= w^0-\frac{\Delta t}{2}pw^1,\\
w^3 &= w^0-\Delta t\,pw^2,\\
w^4 &= w^0-\frac{\Delta t}{6}(pw^0+2pw^1+2pw^2+pw^3),\\
w^{n+1} &= w^4.
\end{aligned} \tag{14}$$

Boundary conditions

The isolated cascade system in Figure 3, shown together with the computational grid, requires inlet, outlet, periodic and wall boundary conditions. At the inlet boundary of the cascade the total enthalpy, total pressure and flow direction are specified while the static pressure is extrapolated from the interior points. At the outlet the static pressure is specified by the back pressure and the other flow quantities such as the density and velocities u and v are again obtained by extrapolation from the interior. On the wall boundary we need only the static pressure. In the rotor region where the finite volumes are collectively moving with the blades, the zero-flux constraint, i.e. $u\mathrm{d}y-v\mathrm{d}x=0$, required for the fixed blade should be relaxed to the moving blade counterpart, $(u-\xi)\mathrm{d}y-(v-\eta)\mathrm{d}x=0$. The flux integral on the wall boundary then takes the form[12]

$$qw|_w=[0,\ p\Delta y,\ -p\Delta x,\ p(\xi\Delta y-\eta\Delta x)]^{\mathrm{T}}. \tag{15}$$

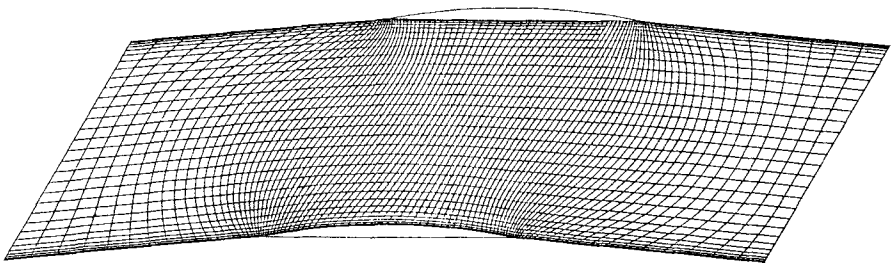

Figure 3. Grid system for isolated cascade flow (H-mesh, 91 × 31)

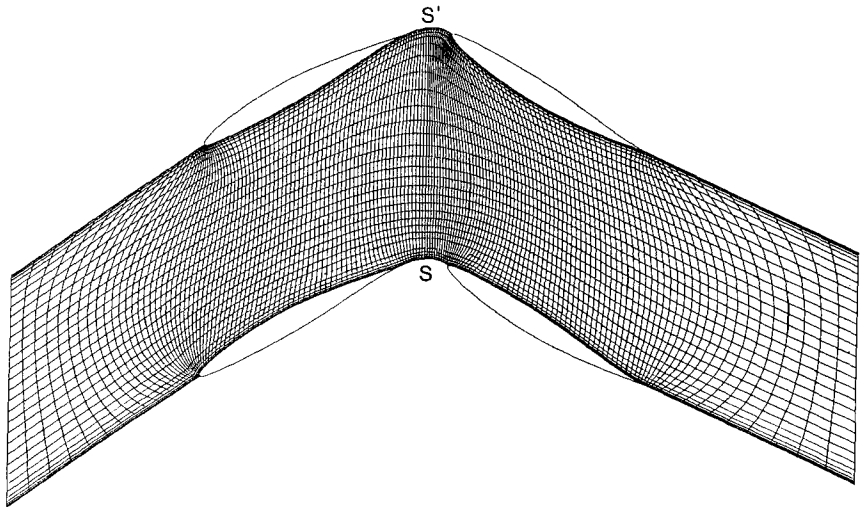

Figure 4. Grid system for compressor stage flow (H-mesh, 156 × 31)

Finally, the wall pressure can be extrapolated from the neighbouring cell by using the equation

$$(x_X^2+y_X^2)p_Y=(x_Xx_Y+y_Xy_Y)p_X+\rho(y_Yu-x_Yv)(x_{XX}v-y_{XX}u), \tag{16}$$

where X and Y represent the local orthogonal streamline co-ordinates. For the rotor blades the same equation can be used by replacing the absolute velocity components u and v by the velocity relative to the moving blades.

For the stator–rotor stage flow analysis the assumption is made here on the cascade configuration that two rows of blades have the same pitch as exemplified in Figure 4. On the sliding surface (S–S′) between the fixed and the moving grid system we used a simple interpolation procedure at each time step. In the present study the two-sliding-grid system worked beautifully since the adjoining boundary (S–S′) was situated in the region where the flow properties had no major gradient.

Application

An elliptic grid generator devised by Steger and Sorenson[13] was used here to produce the grids shown in Figures 3 and 4. Figure 3 consists of an isolated row of blades of 5% semicircular arc aerofoils with 30° stagger angle and unit solidity. We used a 91 × 31 H-mesh system with 51 grid points assigned to the blade. Figure 4 shows the stator–rotor compressor stage with a 156 × 31 H-mesh system. The stator and rotor blades are both NACA 65410 aerofoils with 30° stagger angle and unit solidity; the stator–rotor gap is 20% of the blade chord length.

RESULTS AND DISCUSSION

The present moving grid formulation was first tested for accuracy on an isolated cascade of blades. The pressure contour in the stator passage flow obtained by the fixed grid finite volume method is shown in Figure 5 for an inlet Mach number 0·9713 and inlet flow angle 37·5°. Figure 6 shows the result of an equivalent dynamic blade simulation performed with the moving grid finite volume method. It consists of the same aerofoils with zero inlet flow angle, inlet Mach number

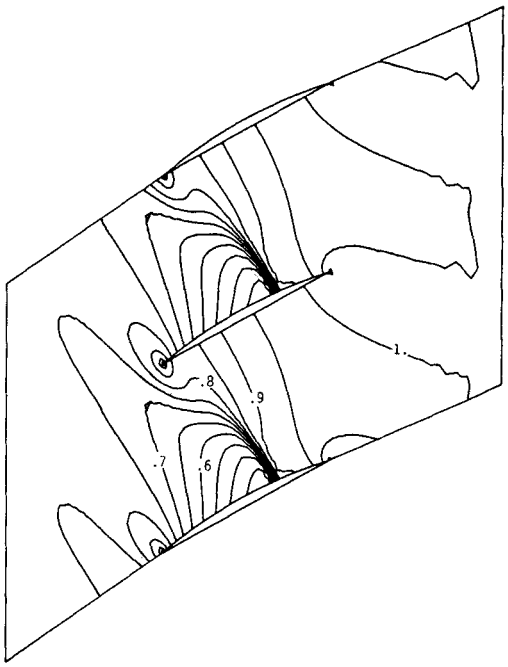

Figure 5. Pressure contour by fixed grid finite volume method, $\Delta(p/p_b)=0{\cdot}05$

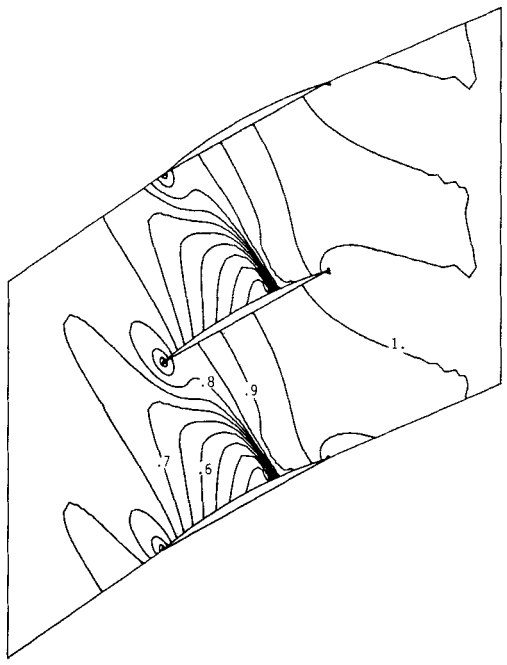

Figure 6. Pressure contour by moving grid finite volume method, $\Delta(p/p_b)=0{\cdot}05$

0·7706 and non-dimensional blade speed −0·6724 in the y-direction. The identical pressure contours in the two different approaches demonstrate that the present moving grid finite volume method is as accurate as the fixed grid counterpart. The total wall pressure loss along the blade is plotted in Figure 7 for the two methods. Generally good agreement is obtained in terms of shock wave strength and location. A minor difference in the oscillation pattern is, however, found in the curve of the total pressure loss upstream of the shock, which evidently does not alter the overall features of the computed flow physics.

The stator–rotor compressor stage flow is now analysed for a stator inlet Mach number 0·8325, stator inlet flow angle 37·5° and non-dimensional vertical rotor blade speed 0·88. The transient behaviour of the force components converging towards the periodic flow is shown in Figure 8. It is seen that, starting from the initial pseudo-steady solution which had been obtained without the surface-sliding effect, approximately two and six cycles of revolution are required for the stator and rotor blades respectively before an apparent periodicity is attained in the axial and tangential force components. Rigorous analysis shows, however, that about 20 cycles are necessary before a purely periodic flow is assumed, which can be demonstrated by the closed phase diagrams in Figure 9. This is in contrast to the five cycles reported for the periodic supersonic stage flow.[5] Figures 8(a), 8(b) and 9(a) clearly indicate that the stator blade maintains near-harmonic axial and tangential forces owing to the cyclic disturbances radiated from the downstream rotors, which may be called 'potential interaction'. In contrast, the rotor blade experiences more complicated subharmonic fluctuations in a period of motion owing to 'inviscid wake–rotor interaction'; see Figures 8(c), 8(d) and 9(b).

Figures 10(a) and 10(b) show the wall pressure distribution on the stator and rotor blade respectively at the moments of maximum and minimum tangential forces. The stator blade experiences a tangential force in the positive y-direction and the rotor blade in the negative y-direction (the direction of force is not shown in the figure). Figures 11(a), 11(b) and 11(c) represent the pressure contours after 0, $\frac{3}{8}$ and $\frac{3}{4}$ cycle respectively. These figures together with Figure 10(a) show that the flow properties in the stator flow passage are virtually unchanged ahead of the shock waves despite the cyclic upstream disturbances from the trailing rotor blades. In the neighbourhood of the leading edge of the dynamic rotor blades the pressure is high enough to cause a transient upstream influence on the stator blades. This upstream influence is propagated up to the shock position in the stator flow passage, about mid-chord of the stator blade on the pressure side and near the trailing edge of the aerofoil on the suction side. This inviscid potential

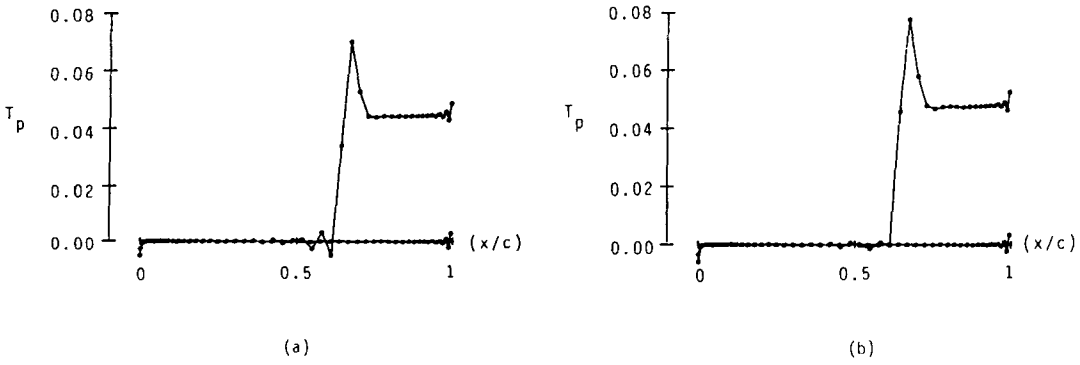

Figure 7. Total wall pressure loss, $T_p=(p/p_\infty)/(\rho/\rho_\infty)^\gamma-1$: (a) fixed grid finite volume method; (b) moving grid finite volume method

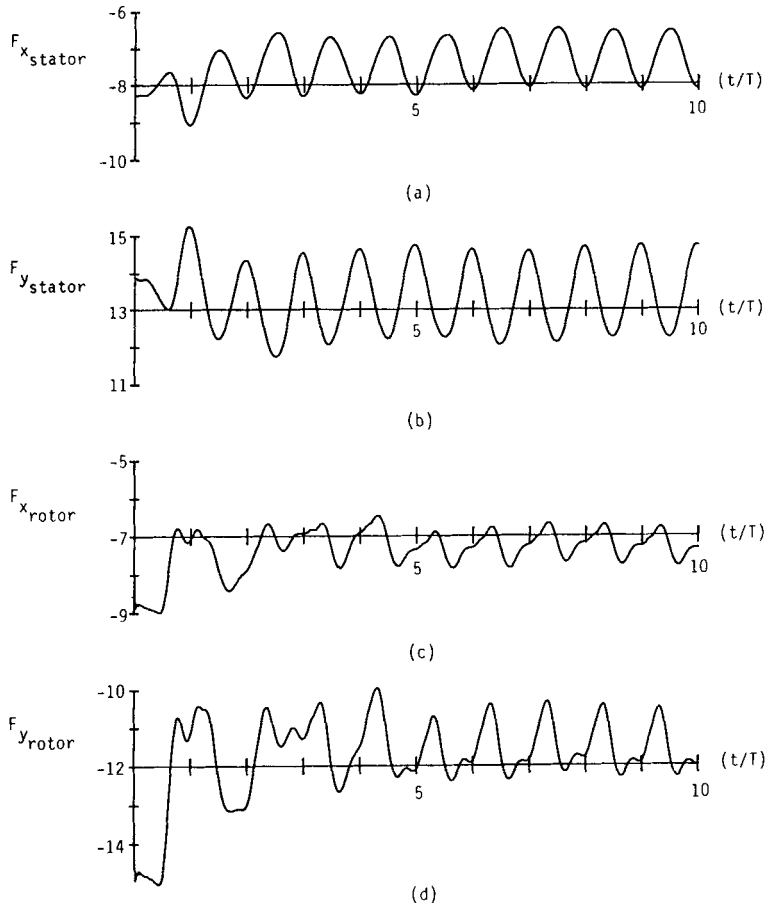

Figure 8. Transient blade force components: (a) stator axial force; (b) stator tangential force; (c) rotor axial force; (d) rotor tangential force

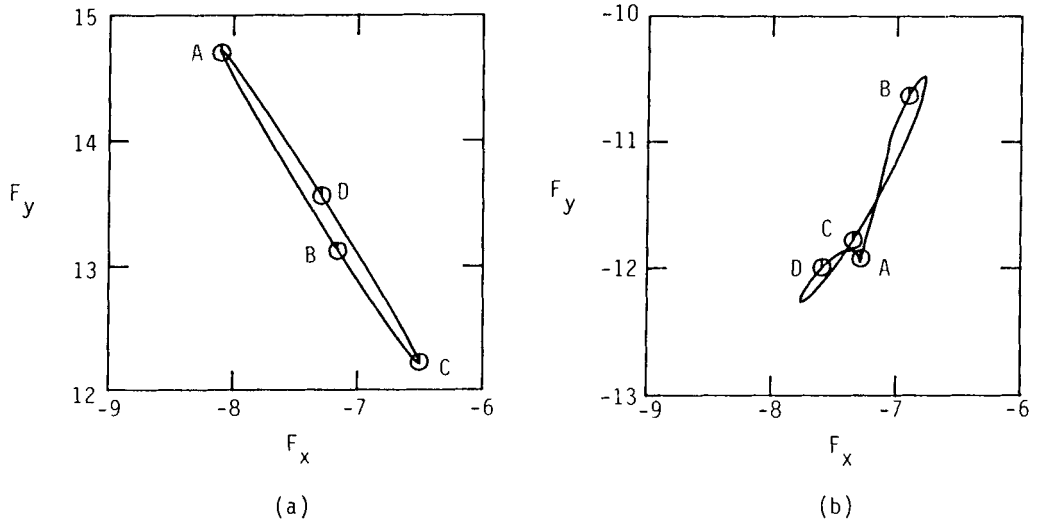

Figure 9. Phase relation of blade forces—point A is at 0, B at $\frac{1}{4}$, C at $\frac{1}{2}$ and D at $\frac{3}{4}$ cycle: (a) stator; (b) rotor

stator–rotor interaction has caused the difference between the maximum and minimum wall pressure curves. The inviscid stator wake–rotor interaction, however, turned out to be relatively small in magnitude, especially for the rotor part; see Figure 10(b). This would not be the case if the flow had been viscous.[4] The unsteady subharmonic fluctuation of the force coefficients on the rotor is, however, believed to be due to this particular interaction.

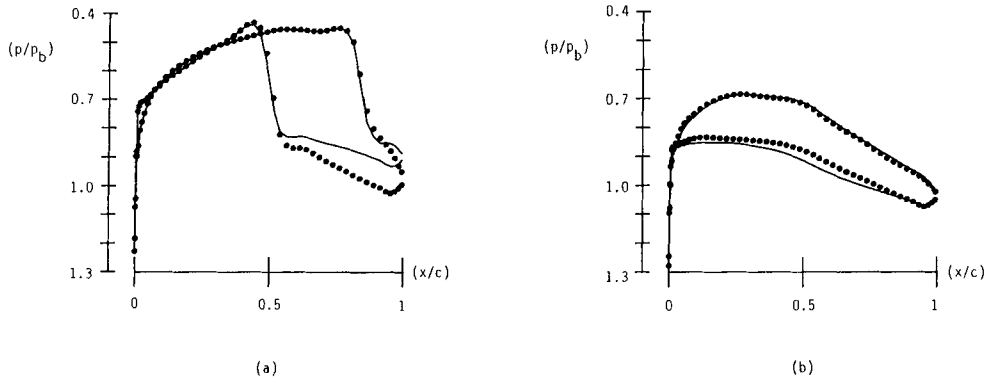

Figure 10. Wall pressure curves at the instant of maximum (·····) and minimum (——) tangential forces: (a) stator; (b) rotor

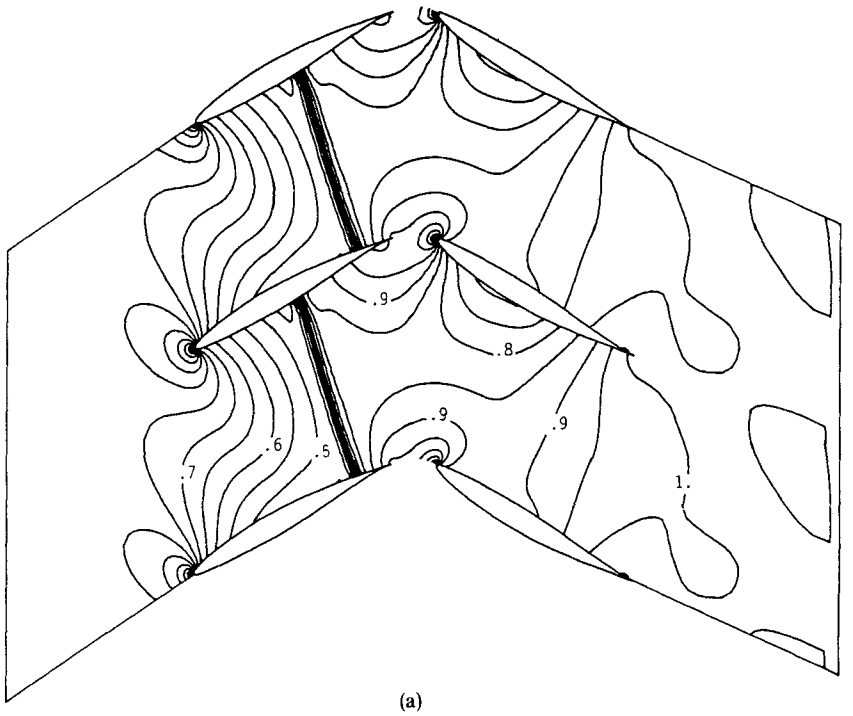

(a)

Figure 11(a)

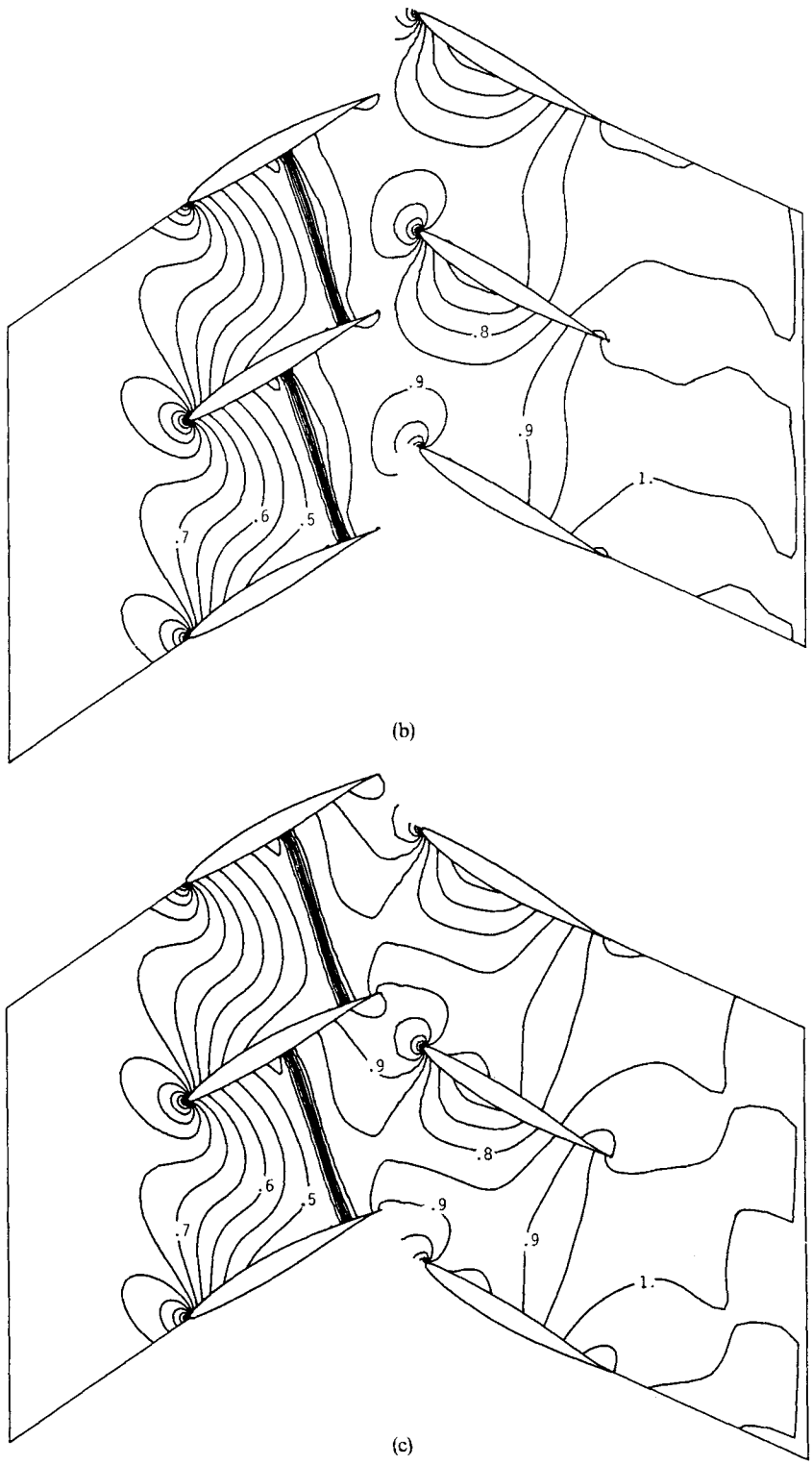

Figure 11. Pressure contours at various cycle phases, $\Delta(p/p_b)=0{\cdot}05$: (a) at 0, (b) at $\frac{3}{8}$ and (c) at $\frac{3}{4}$ cycle

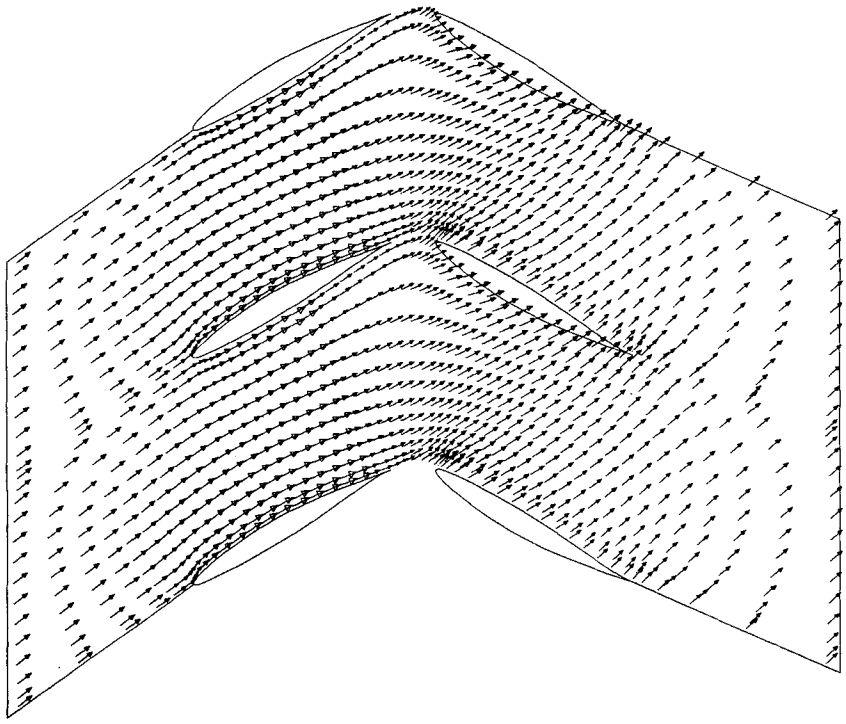

Figure 12. Instantaneous velocity vectors in compressor stage flow

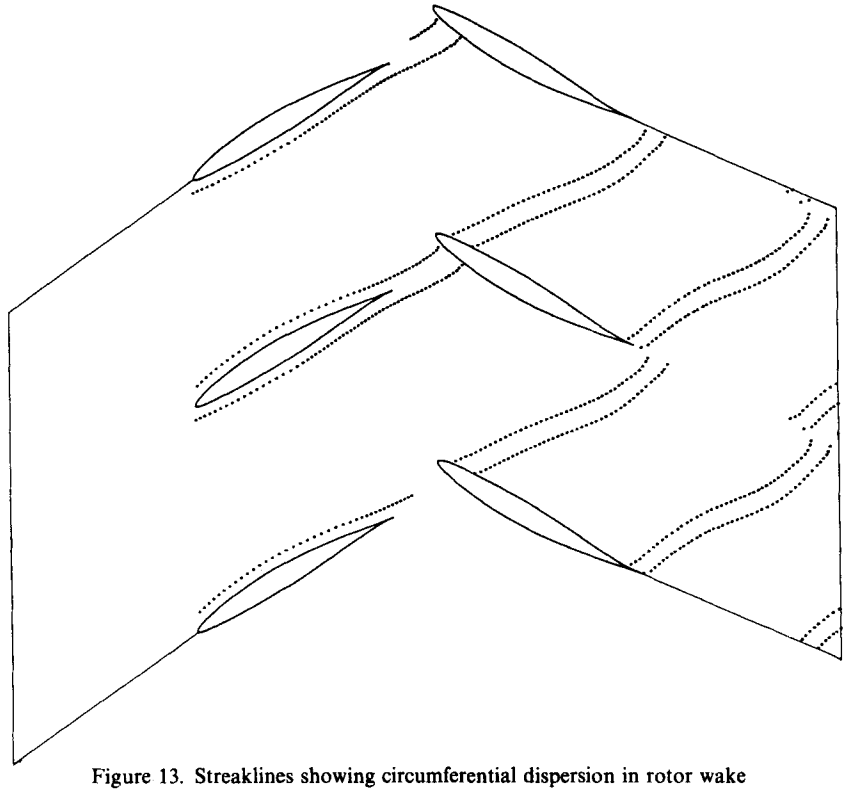

Figure 13. Streaklines showing circumferential dispersion in rotor wake

Figure 12 depicts the instantaneous velocity vectors in the compressor stage flow. The flow accelerated on the suction side of the stator blade is quite slowed down by a sudden, nearly normal shock wave. At the exit the flow is pressurized to the level of the back pressure by the work transmitted from the rotor blades. The rotational flow passed through the stator passage is intercepted by the rotor blades as shown in Figure 13 by the streaklines. The different degree of flow acceleration between the suction side and the pressure side of the moving rotor blade causes the circumferential flow dispersion in the wake of the rotor blades. This phenomenon, occurring always in the compressor stage flow, depends on the blade configuration, blade loading and aerodynamic force coefficients.[14] The viscous effect in a real fluid flow would, however, introduce flow separation and a mixing mechanism of the turbulent diffusion, thus altering the scene of the compressor passage flow further.

CONCLUSIONS

A generalized finite volume method treating the stator and rotor regions with similar formulations is presented to solve the Euler equations for transonic compressor stage flow. The adjoining of the present moving grid finite volume method with the existing fixed grid counterpart by interpolative data exchange at the sliding surface has worked quite efficiently. The calculated results have explained the mechanism of potential interaction between the stator and rotor blades and the inviscid wake–rotor interaction. It is also indicated that some of the above results would be altered in a more complicated way if the viscous effect of a real fluid were to be taken into account.

ACKNOWLEDGEMENT

This work was partially supported by the Korea Science and Engineering Foundation under Grant No. 860301.

REFERENCES

1. M. B. Giles, 'Calculation of unsteady wake/rotor interactions', *AIAA Paper 87-0006*, 1987.
2. J. Chauvin, C. Sieverding and H. Griepentrog, 'Flow in cascades with a transonic regime', in L. S. Dzung (ed.), *Flow Research on Blading*, Elsevier, Amsterdam, 1970, pp. 151–196.
3. J. I. Erdos, E. Alzner and W. McNally, 'Numerical solution of periodic transonic flow through a fan stage', *AIAA J.*, **15**, 1559–1568 (1977).
4. P. C. E. Jorgenson and R. V. Chima, 'Explicit Runge–Kutta method for unsteady rotor/stator interaction', *AIAA J.*, **27**, 743–749 (1989).
5. M. M. Rai, 'A relaxation approach to patched-grid calculations with the Euler equations', *AIAA Paper 85-0295*, 1985.
6. M. M. Rai, 'Navier–Stokes simulations of rotor–stator interaction using patched and overlaid grids', *AIAA Paper 85-1519*, 1985.
7. M. M. Rai, 'Unsteady three-dimensional Navier–Stokes simulations of turbine rotor–stator interaction', *AIAA Paper 87-2058*, 1987.
8. J. T. Oden, T. Strouboulis and Ph. Devloo, 'Adaptive finite element methods for high-speed compressible flows', *Int. j. numer. methods fluids*, **7**, 1211–1228 (1987).
9. A. Jameson, W. Schmidt and E. Turkel, 'Numerical solutions of the Euler equations by finite volume methods using Runge–Kutta time stepping schemes', *AIAA Paper 81-1259*, 1981.
10. K. Karamcheti, *Principles of Ideal-Fluid Aerodynamics*, Wiley, New York, 1966.
11. T. H. Pulliam, 'Artificial dissipation models for the Euler equations', *AIAA J.*, **24**, 1931–1940 (1986).
12. A. Lerat and J. Sidès, 'A new finite-volume method for the Euler equations with applications to transonic flows', in P. L. Roe (ed.), *Numerical Methods in Aeronautical Fluid Dynamics*, Academic Press, New York, 1982, pp. 245–288.
13. J. L. Steger and R. L. Sorenson, 'Automatic mesh-point clustering near a boundary in grid generation with elliptic partial differential equation', *J. Comput. Phys.*, **33**, 405–410 (1979).
14. D. C. Wisler, R. C. Bauer and T. H. Okiishi, 'Secondary flow, turbulent diffusion, and mixing in axial-flow compressors', *ASME J. Turbo.*, **109**, 455–482 (1987).